Chapter 2

Experimental procedure and characterization techniques

2.1 Sample synthesis

The physical properties of the materials are highly sensitive to their crystallographic structures. On an atomic level, the structure implies the arrangement of the atoms relative to each other. In crystalline materials, the atoms exhibit a regular and periodic arrangement, which leads to a macroscopic (long-range) crystal structure of the materials. In addition to long-range ordering, there exists short-range ordering, and sometimes the long-range structure is considered to be driven by the ordering (partial or complete) in components of short-range atomic arrangements (*e.g.,* $BaTiO_3$ [2, 103]), which plays a crucial role in the determination of most of the physical properties of such material. In order to have an idea about the correlation between the crystallographic structure and physical properties, the synthesized ceramic system needs to be subjected to various characterization techniques. Therefore, a clear understanding of structure-property correlations needs well-synthesized samples. Thus the preliminary step for various experimental characterizations is the synthesis of good-quality samples. There are various ways of synthesis of samples. One of

them, which is very common, is named as the solid-state reaction method, and many of the perovskite-based ceramic systems are synthesized using this method. In the present study, we have used the solid-state reaction method for the synthesis of samples.

2.1.1 Solid-state reaction method

The solid-state reaction method is a common method used for the synthesis of polycrystalline materials by using solid reagents [209]. The starting point of the solid-state reaction method lies in the mixing of raw materials. There are various ways of mixing. Sometimes the raw materials are placed in ethanol media and, thereafter, it is mixed with Agate mortar and a pestle. On the other hand, the ball milling technique is also used for the mixing. In

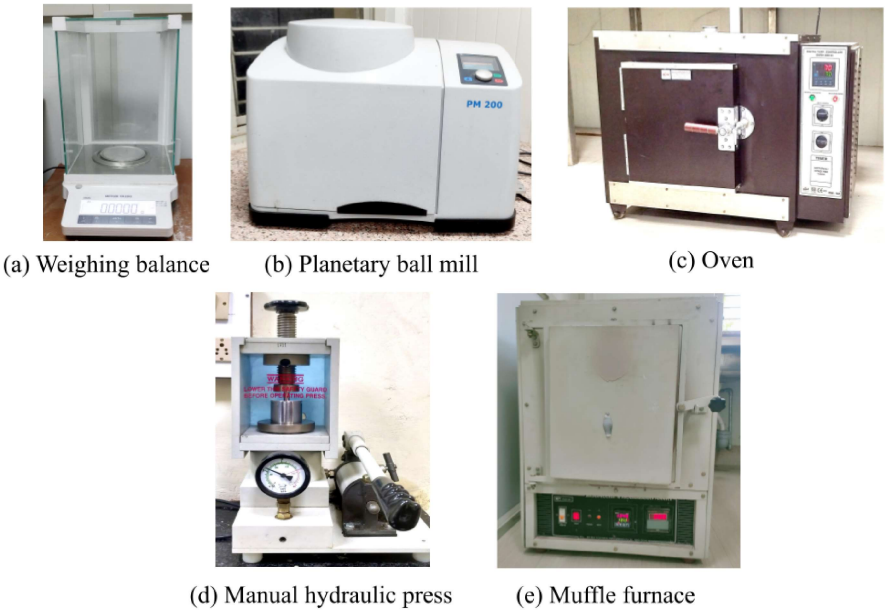

Fig. 2.1 The instruments used in the synthesis of samples via solid-state reaction method.

the present study, this technique was used, where the raw materials were placed in zirconia zar with zirconia balls in ethanol media. In this study, a planetary ball mill (Retsch model PM 200) has been used for the crushing, grinding, and mixing of the starting materials. Thereafter the obtained slurry is dried, and milled powders are separated from the balls

and then subjected to heat treatments. First of all, the mixed powders were calcined in the alumina crucibles at high temperature in the programmable Muffle Furnace capable of going up to 1400 ^{0}C, and thereafter the calcined powders were mixed with 2 wt % PVA (polyvinyl alcohol) acting as a binder and then pelletized in the form of discs. Thereafter the sintering of the green pellets was carried out in the Muffle Furnace at a temperature higher than the calcination temperature. The various instruments used in the synthesis of samples via solid-state reaction method are shown in Fig. 2.1. After synthesis, the samples were subjected to various characterizations, as mentioned below.

2.2 Characterization techniques

In order to analyse the correlation of the physical properties of the synthesized ceramics with their crystallographic phases and to predict the suitability of the materials for various applications, the synthesized ceramics has been subjected to characterization techniques discussed here.

2.2.1 X-ray diffraction method

The determination of crystal structure is a key point for the complete understanding of the properties of materials. In this regard, X-ray crystallography has remained one of the major tools. The underlying principle is that the atoms present in the crystalline materials cause X-ray beams to diffract in a variety of specific directions. When a periodic waveform interacts with an ordered array of atoms, it gets diffracted by the crystalline material (see Fig. 2.2). The scattered waves gets emitted from the atoms located at different positions; hence either constructive or destructive interference takes place in different directions, and the maxima in the intensity occur when the geometric condition given below is satisfied

[210].

$$2d_{hkl}sin\theta = \lambda \quad (Bragg's\ law) \tag{2.1}$$

here d_{hkl} stands for interplanar spacing, λ is the incident ray's wavelength, θ is the Bragg angle which the incident ray makes with the plane, and hence 2θ is the angle between the incident (direct) and the transmitted beam. The spacing between the corresponding planes (d_{hkl}), from which X-rays are reflected, characterizes the X-ray diffraction spectra and determines the positions of the peaks in terms of 2θ [210]. The patterns of the reflecting planes $\{hkl\}$ provide the details about the crystal's space group [211]. Thus a strong relationship exists between the atomic arrangement and the diffraction pattern of the material. Therefore, the diffraction peak positions and its intensity reveals information about the unit cell parameters, atomic positions, thermal parameters, etc. [212].

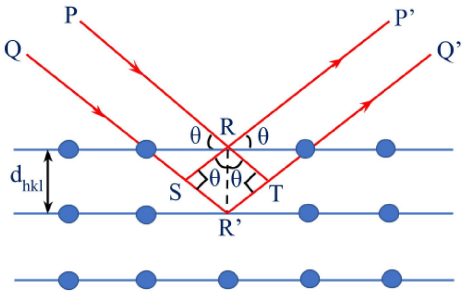

Fig. 2.2 Representation of X-ray diffraction by a crystal.

To analyse the crystallographic phase and purity of the synthesized ceramics, the powder X-ray diffraction measurements were performed on a 9 kW rotating anode based Rigaku SmartLab high-resolution X-ray diffractometer (see Fig. 2.3), operated in Bragg–Brentano geometry. The X-ray diffraction data have been collected over the 2θ range 20^0 to 120^0 with a step size of 0.02, using Cu-$K_{\alpha 1}$ (1.54059 Å) radiation. The data were recorded in a continuous scan mode. In order to fix the crystallographic structure of the various synthesized ceramics, we have performed the Rietveld refinements of the X-ray diffraction patterns using the FULLPROF package [213].

Rietveld refinement

Rietveld refinement is an innovative and widely used method for analysing the structure of the materials using powder diffraction data. It is based on the simple idea of refining the crystal structures, employing intensities and positions of the diffraction peaks [214]. Using this method, the structural analysis, including lattice parameters, atomic coordinates, thermal vibrations (isotropic and anisotropic), etc., can be refined. In addition, this technique can also be used to probe local off-centered displacements existing in the materials [14, 215]. In order to fit the data, the Rietveld method utilizes a model, and if the model is accurate, then it gives rise to intensity values corresponding to the observed diffraction pattern. The Rietveld algorithm optimizes the model function to minimize the quantity $\Sigma_i \, w_i[y_i(\text{obs})-y_i(\text{calc})]^2$, where y_i(obs) is the observed intensity at step i, y_i(calc) denotes the calculated intensity, and w_i corresponds to a suitable weight associated to each observed intensity (usually equal to $\frac{1}{y_i(obs)}$). The y_i(calc) is described by analytical functions, which depends on structural and profile parameters, *viz.*, atomic positional coordinates, lattice parameters, occupancies, peak width, peak shape, background, zero-shift error, sample displacement, preferred orientation, etc. [214]. All these parameters are refined by the method of least squares [214]. Since there are a number of refinable parameters, the minimization process may sometimes lead to false minima or can diverge. These possibilities can be avoided by using the starting structural model

Fig. 2.3 Rigaku SmartLab high-resolution X-ray diffractometer.

(calculated) as close as possible to the observed one [214]. In addition, the proper modeling of background using appropriate function and the use of high-quality diffraction patterns also helps in order to avoid the false minima in the refinements. While performing the refinements, one has to observe at each cycle that the refinement is going in the right direction until the best fit between the observed and simulated diffraction pattern is achieved. The goodness of fit between the observed and calculated pattern can also be described mathematically in terms of the agreement factors or R values, given below

$$R_{wp} = \left\{ \frac{\sum_i w_i [y_i(\text{obs}) - \text{y}_\text{i}(\text{calc})]^2}{\sum_i w_i [y_i(\text{obs})]^2} \right\}^{1/2} \tag{2.2}$$

$$R_{exp} = \left\{ \frac{N - P}{\sum_i^N w_i y_i(\text{obs})^2} \right\}^{1/2} \tag{2.3}$$

In the above expressions, N denotes the number of data points, and P is the number of parameters. Generally, the best fit is considered as the one when R_{wp} is close to the R_{exp}. There, is also another parameter termed "chi squared", defined as the square of the ratio of R_{wp} and R_{exp}, is used to judge the goodness of fit,

$$\chi^2 = \left(\frac{R_{wp}}{R_{exp}} \right)^2 \tag{2.4}$$

This parameter is frequently quoted in the literature and should approach 1 for the best fit [216]. Although these parameters can be used to judge the quality of the refinement but it is important to avoid overinterpreting them. The most crucial criterion to judge a Rietveld refinement's quality is the fitting between the observed and calculated patterns and the chemical sense of the structural model obtained after the best fit [216, 217].

2.2.2 Dielectric measurement

Dielectric materials are more or less insulators, which are polarizable, *i.e.,* either it contains dipoles or can produce them when an external electric field is applied. When the dielectric materials are exposed to an external electric field, the separation of charges takes place within the elementary volume of the material, but the overall dielectric material stays neutral. Under the influence of an electric field, the positive charges get displaced in the field's direction, and the negative charges towards a direction opposite to that of the applied field. Based on the variation in polarization as a function of the electric field, dielectric materials are classified into two categories, *viz.,* linear dielectrics and non-linear dielectrics. A linear dielectric system is characterized as one whose dielectric constant is independent of the electric field, and the polarization exhibits a linear behaviour as a function of electric field [5, 218], given by the following equation

$$P = \varepsilon_0 E \chi \tag{2.5}$$

$$\chi = \varepsilon_r - 1 \tag{2.6}$$

here, P stands for the polarisation of the dielectric material, ε_0 (= 8.854×10^{-12} F/m) for the permittivity of the free space, E for the applied electric field, χ for the electric susceptibility, and ε_r is termed as relative dielectric constant ($\varepsilon_r = \varepsilon/\varepsilon_0$), which corresponds to the ratio between the material's permittivity (ε) to that of free space (ε_0) [5]. On the other hand, the non-linear dielectrics are those whose polarization increases to a maximum value (P_{max}) as the electric field increases (charging process), and thereafter, with the lowering of the electric field, it decreases with the polarization being non-zero (remnant polarization; P_r) for the zero electric field (discharging process) [218, 219]. The linear dielectric materials exhibit low ε_r values due to the absence of spontaneous polarization [5, 219]. However, the non-linear dielectric materials (ferroelectric, antiferroelectric,

relaxor ferroelectrics, and relaxor antiferroelectrics) exhibit fascinating physical properties, which makes them suitable for a wide variety of applications [5, 218].

When an alternating electric field is applied to the dielectric material, the resulting polarization alternates its direction as a function of the field. If the frequency of the applied field is sufficiently high, then there is a lag between the orientation of the permanent dipole and the field direction. In such a case, the electric field vector (E) and the electric displacement vector (D) experience a phase difference given by the following equation

$$E = E_0 e^{i\omega t} \tag{2.7}$$

$$D = D_0 e^{i(\omega t - \delta)} \tag{2.8}$$

here, E_0 and D_0 correspond to the amplitudes of the respective quantities. As per the equation

$$D = \varepsilon E \tag{2.9}$$

$$D_0 e^{i(\omega t - \delta)} = \varepsilon^* \varepsilon_0 E_0 e^{i\omega t} \tag{2.10}$$

where ε^* represents the complex dielectric permittivity given as

$$\varepsilon^* = \varepsilon' - i\varepsilon'' \tag{2.11}$$

here, ε' and ε'' corresponds to the real and imaginary part of dielectric permittivity. The imaginary part, *i.e.,* ε'' is also referred to as the dielectric loss of the materials. Thus using equations (2.10) and (2.11), ε' and ε'' can be expressed as

$$\varepsilon' = \frac{D_0}{\varepsilon_0 E_0} \cos\delta \tag{2.12}$$

and

$$\varepsilon'' = \frac{D_0}{\varepsilon_0 E_0} \sin\delta \tag{2.13}$$

these two equations give rise to

$$\tan\delta = \frac{\varepsilon''}{\varepsilon'} \tag{2.14}$$

where the quantity $\tan\delta$, *i.e.,* loss tangent (dissipation factor), is described as the ratio of

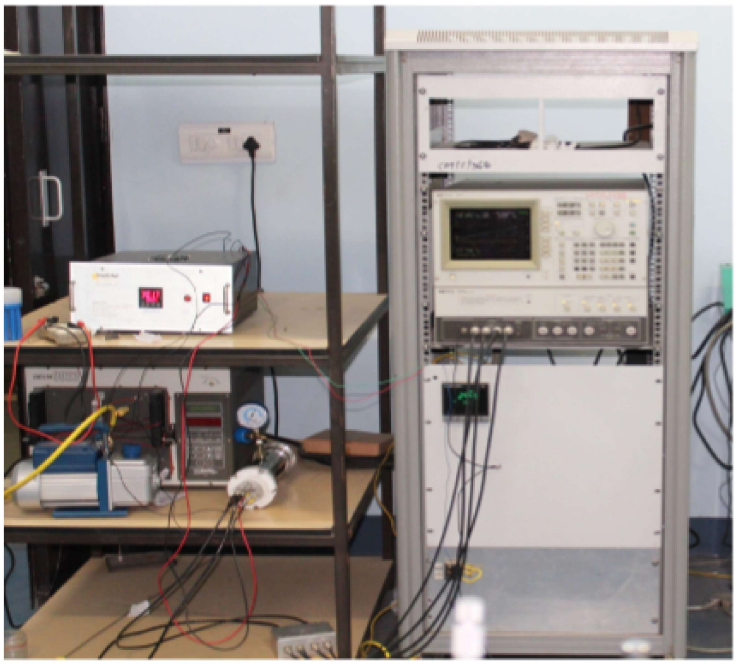

Fig. 2.4 Impedance analyser used for dielectric measurements.

dissipated energy and stored energy per charging cycle. In the present studies, we have performed the temperature-dependent dielectric measurement at various frequencies using HP4194A impedance analyzer (see Fig. 2.4) with a heating rate 2 ^{0}C/min.

2.2.3 Polarization *vs.* Electric field (PE) hysteresis loop measurements

The total dipole moment present in a dielectric material per unit volume is referred to as electric polarization. This polarization in the dielectric material induces an internal electric

field (E_{ind}) directed opposite to the external electric field (E_{ext}), and thus the net electric field inside the dielectric material becomes

$$E_{net} = E_{ext} - E_{ind} \tag{2.15}$$

Thus the resultant electric field (described as the negative gradient of scalar potential) experienced by the dielectric material is decreased, and therefore the voltage decreases. The decrease in voltage improves the capacitance ($C = \frac{Q}{V}$) of the material, which is the requirement for energy storage applications [5]. The energy-storing capacity of the dielectric materials is well studied by measuring their polarisation *vs.* electric field (PE) hysteresis loop. Except for the linear dielectrics, all other dielectrics exhibit their characteristic PE

Fig. 2.5 Polarization *vs.* electric field (PE) hysteresis loop tracer.

hysteresis loop. For example, ferroelectric materials are generally characterized by their square shape PE hysteresis loop, while relaxor ferroelectrics exhibit a slim PE hysteresis loop. On the other hand, antiferroelectric materials show a double hysteresis loop, and the relaxor antiferroelectric also exhibits a loop similar to antiferroelectrics, but it becomes nar-

row [219]. Further, in non-linear dielectric materials, the energy stored during the charging cycle can not be completely released during discharging, and some energy loss occurs [219]. Thus to predict the energy-storing capacity of dielectrics, the PE loop measurement is a very useful tool. In the present study, the polarization *vs.* electric field (PE) hysteresis loop measurements have been performed using Radiant Technology's Precision Material Analyzer Workstation based on the virtual ground system (see Fig. 2.5).

2.2.4 Raman spectroscopic measurements

The phenomenon of light interacting with matter serves as the foundation for Raman spectroscopy [220]. Generally, when light interacts with matter, the oscillating electromagnetic field associated with the radiation generates a perturbation in the charge distribution of the materials, which may lead to the exchange of energy and momentum, leaving the state of the materials in a modified form. When an incoming photon interacts with the matter, it may suffer elastic or inelastic scattering. If there is no change in energy of the photon after scattering, then it is called elastic scattering, while if the energy of the photon changes, inelastic scattering occurs. Further, if the light suffers an elastic scattering, it is called Rayleigh scattering. On the other hand, if inelastic scattering occurs, then the phenomenon is called the Raman effect. The Raman effect was experimentally observed in 1928 by an Indian scientist Sir C. V. Raman, for which he was awarded by Noble prize in 1930. The molecules are left in altered vibrational states as a result of this inelastic scattering. In crystalline lattices, the transfer of energy leads to a quantum of lattice vibration known as phonon. The following equation describes the shift in scattered light's angular frequency

$$\omega_{scat} = \omega_p \pm \omega_{osc} \tag{2.16}$$

where ω_{scat} corresponds to scattered light, ω_{osc} represents lattice vibrations, and ω_p denotes the incident photon. If the scattered photon has smaller energy than the incident one, the process is called Stokes-Raman scattering. On the other hand, if the scattered photon has higher energy than the incident one, the process is known as anti-Stokes Raman scattering. In addition, the Raman process must also conserve the momentum as given by the following equation

$$\overrightarrow{k}_{scat} = \overrightarrow{k}_{p} \pm \overrightarrow{k}_{q} \tag{2.17}$$

Here, $\overrightarrow{k}_{scat}$ and $\overrightarrow{k}_{p}$ represents the wave vectors of scattered and incident light while $\overrightarrow{k}_{q}$ corresponds to the wave vector of molecular vibrations or phonons.

As mentioned above, when the molecules and crystals are subjected to an externally applied field, their charge distribution gets perturbed, but only in accordance with the molecule or crystal's symmetry to produce dipoles, which may be anisotropic. This anisotropic property exhibited by molecules and crystals is referred to as polarizability and dielectric susceptibility, respectively. According to the classical theories, the phenomenon of the Raman effect corresponds to the change in polarizability (for molecular vibrations) or dielectric susceptibility (for crystal lattice vibrations) due to the oscillatory nature of their interatomic displacements [221]. The Raman scattering depends on the direction and polarization of the incident light, the crystal symmetry, orientation of the solid sample, and it also depends on the direction and polarization of the scattered light [222]. Typically, the measured Raman spectrum of a material consists of several peaks, which corresponds to the intensity and wavenumber of the Raman scattered light. These peaks are associated with a specific molecular bond vibration, and typically the Raman spectra exhibit a distinct chemical fingerprint for a given material or molecule. In this way, this technique is widely used for the determination of the crystal structures, *e.g.,* complex crystallographic phases driven by octahedral rotations, polar displacements of the cations, etc. [97, 189, 223, 224]. In addition to the global structure determination, it has also been identified as a versatile

Fig. 2.6 Renishaw InVia Raman spectrometer.

technique to probe the local disorder present in the materials due to its capability to detect the atomic arrangements existing over a few unit cells [225, 226, 227]. In this thesis work, we have used the Raman spectroscopy technique to probe the global and local structures. The room temperature Raman spectra of the synthesized samples have been collected via Renishaw InVia Raman spectrometer (Wotton-under-Edge, UK) by using a 532 nm diode-pumped solid-state laser. The resolution of the used Raman spectrometer is $\sim$ 1 cm^{-1}.

2.2.5 Microstructural measurement

The macroscopic properties of the ferroelectric materials depend highly on grains and the structure inside the grains. When the grains are present, then the spontaneous polarization generally becomes discontinuous at the grain boundaries and consequently leads to the depolarizing field. At the same time, the deformation in the unit cell associated with the spontaneous polarization generates an internal stress field in the material due to mechanical constraints imposed on the grains by their neighbours. Therefore, in order to reduce depolarization and elastic energies, spontaneous polarization often leads to the formation

of domains in the grains. These domains possess a complex topology and exhibit various unexpected phenomena [228]. The domains are formed in the ferroelectric polycrystals as a consequence of long-range elastic and electrostatic interactions between the various grains and (or) domains [229]. The domains exhibit a spontaneous polarization along a direction consistent with the symmetry present in the material. Adjacent domains are separated by an interface (width $\sim$ 1-10 nm) having homogeneous nature, termed as domain walls [229]. As the electric field is applied, which is not parallel to domain walls, the domain wall motion occurs, and consequently, it moves, resulting into a global deformation of the shape. Microscopically it refers to the phenomenon where some of the polar vectors near domain walls switch their polarization, and therefore depending on the direction of the applied field, some of the domains grow/shrink in size. The switching of the dipoles (polarization vector) and deformation in shape due to domain wall motion leads to the extrinsic contributions in the dielectric, and piezoelectric properties of the materials [230]. Thus one can see that, based on the microstructural features, various physical properties of the material gets affected. In this thesis work, the microstructural observations were performed using a high-resolution scanning electron microscope (HR-SEM: Nova Nano SEM 450, FEI Company of USA (S.E.A.) PTE, LTD) which is shown

Fig. 2.7 High-resolution scanning electron microscope.

in Fig. 2.7, in order to observe the effect of dopants in grain size, and distribution of grains to assist the measured physical responses.